Analysis of Diffusion at Buried Interfaces Following Area-Selective Atomic Layer Deposition For Dopant-Containing Small Molecule Inhibitors

by

Robert Norden

A thesis submitted to the Faculty of the University of Delaware in partial fulfillment of the requirements for the degree of Bachelor of Science in Chemical Engineering with Distinction

Spring 2025

Analysis of Diffusion at Buried Interfaces

Following Area-Selective Atomic Layer Deposition

For Dopant Containing Small Molecule Inhibitors

by

Robert Norden

Approved: 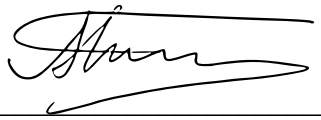

Andrew Teplyakov, Ph.D.
Professor in charge of thesis on behalf of the Advisory Committee

Approved: 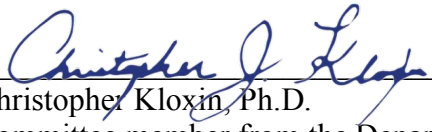

Christopher Kloxin, Ph.D.
Committee member from the Department of Chemical and Biomolecular Engineering

Approved: 

Zhihao Zhuang, Ph.D.
Committee member from the Board of Senior Thesis Readers

Approved: _____

Sarah Trembanis, Ph.D.
Chair of the University Committee on Student and Faculty Honors

ACKNOWLEDGMENTS

I would like first and foremost to thank my parents for supporting me through my time at college. I know it could not have been easy raising three kids and funding them through the beginning of their lives. I will be eternally grateful. I would also like to thank everyone in the Teplyakov research group for giving me the opportunity to study a subject as amazingly beautiful as physical chemistry. Lastly, to all my friends and colleagues within the college of engineering and beyond, none of this could have been possible without you.

TABLE OF CONTENTS

LIST OF TABLES

LIST OF FIGURES

ABSTRACT

With further scaling of transistors to the sub-5 nm regime, photolithography is becoming less feasible in favor of bottom-up methods such as area-selective atomic layer deposition (AS-ALD). This thesis reports on the investigation of 4-fluorophenylboronic acid (FPBA) as a small molecule inhibitor (SMI) for selective doping at buried interfaces. Titania thin films were deposited on silicon substrates functionalized with FPBA and subsequently subjected to a variety of thermal treatments including both vacuum tube furnaces and rapid thermal annealing (RTA). Characterization methods, such as XPS, AFM, SEM, ellipsometry and ToF-SIMS were employed to assess surface integrity, dopant preservation and depth profiles. Diffusion was modeled using simple one-dimensional Fickian diffusion with an Arrhenius-type temperature-dependent diffusion coefficient. Through the experiments, it was found that boron preferentially diffused into the titania as opposed to the silicon, with fitted Gaussian profiles showing a finite amount of broadening for both annealing processes. However, for multiple experiments, intensive thermal load resulted in significant enough surface damage to compromise the quantification of some samples. Low heat RTA anneals preserved surface quality and led to controlled, albeit slow diffusion, showing the sensitivity of the process. This work presents a proof-of-concept for the incorporation of area-selective surface chemistry with monolayer doping techniques and reveals the tradeoffs involved in process tuning.

Chapter 1

Introduction

1.1 Motivation for Area-Selective Atomic Layer Deposition

The invention of computers has had profound impacts on modern society, and since their invention there has been tremendous pressure to increase their spatial efficiency. The primary method of doing this has been to miniaturize the space each transistor occupies on a given integrated circuit. The pace of miniaturization is best visualized in Moore's law where the number of transistors on a given circuit is estimated to double every year [12]. While advances in size reduction have slowed since Moore's 1965 prediction, companies such as Taiwan Semiconductor Company are currently producing 3nm technology with plans to release 2nm technology in the future [17]. At these scales, the conventional top-down methods of transistor construction will no longer be viable, necessitating the development of bottom-up technologies.

One potential candidate for the manufacturing of these devices is area-selective atomic layer deposition (AS-ALD), which is a self-limiting process in which sequential cycles of precursors are dosed to grow thin films. When combined with certain resists or substrates such as self-assembled monolayers (SAM) or small molecule inhibitors (SMI), the growth can be limited to only areas of interest (growth areas) and inhibited in others (non-growth areas). This process is shown in figure 1.

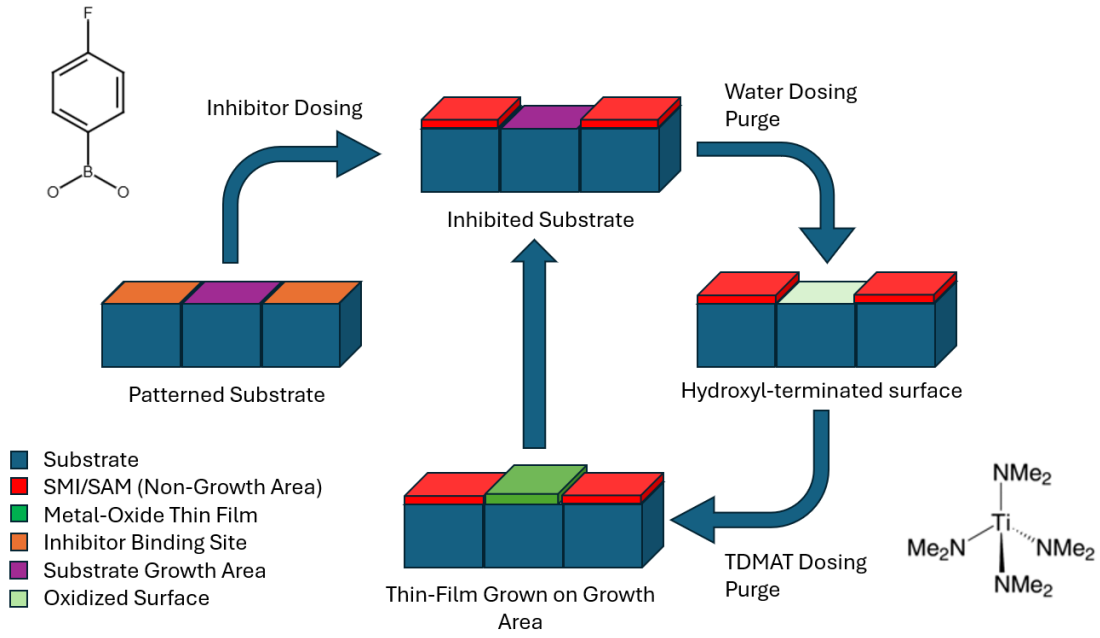

Figure 1: AS-ALD Schematic using TDMAT/H_2O as precursors and FPBA as an inhibitor

1.2 Motivation for Study

Although AS-ALD is a very promising method for achieving bottom-up fabrication, the selectivity between growth and non-growth areas can degrade over many cycles. This can be caused by many reasons, including but not limited to defects, oxidation, and incomplete coverage. When selectivity is lost, many may choose to etch the film to remove the overgrown layer, often done using atomic layer etching, and redeposit using ALD to maintain selectivity [16]. However, if the blocking layer used for AS-ALD contained a dopant molecule, then the overgrown layer could be used as a capping layer for monolayer doping. This would potentially allow for area-selective monolayer doping in just the non-growth area. A schematic of the proposed process can be found in figure 2.

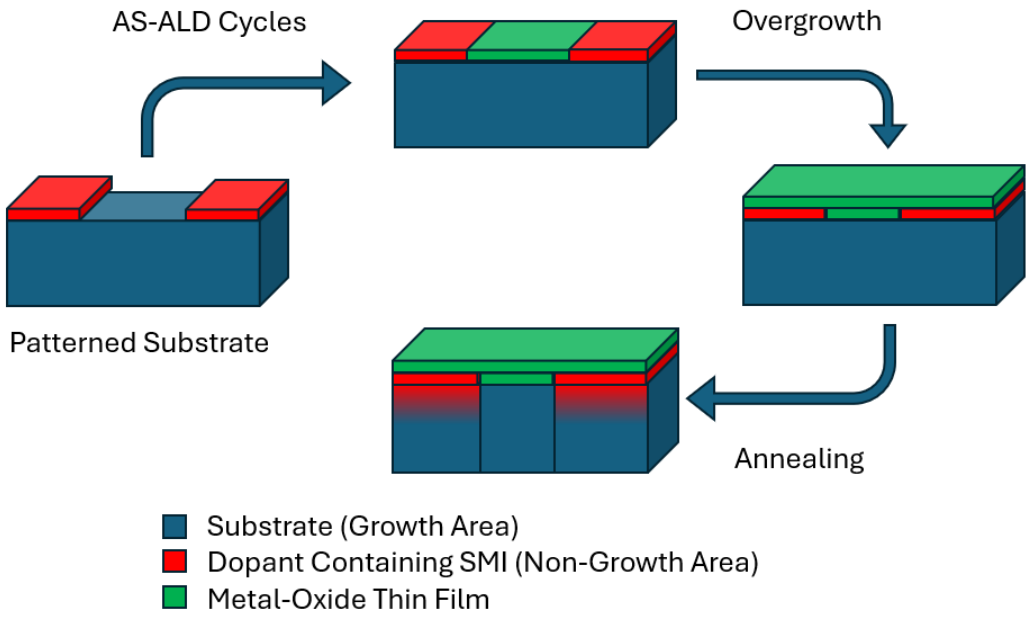

Figure 2: Proposed process for area-selective doping

To study this potential, 4-fluorophenylboronic acid (FPBA) was used as a small molecule inhibitor as it has been previously used within the group as an ALD resist [15]. Titania will be used as the metal-oxide thin film, and the distribution of fluorine and boron following thermal treatment of the titania-overgrown FPBA-modified surfaces will be used as a model for the work presented in this thesis.

Chapter 2

Methods

2.1 Preparation of hydrogen-terminated Si (100) and hydroxyl-terminated Si (100)

Si (100) wafers were cleaned via a modified Radio Corporation of America procedure outlined in a paper by Werner Kern. Teflon beakers were initially cleaned using a solution of Milli-Q water, hydrogen peroxide, and ammonium hydroxide in a 4:1:1 volume ratio for 30 minutes on an 80°C water bath. This mixture is known as the standard cleaning-1 (SC-1) solution. Next, silicon wafers were cleaned with yet another freshly prepared SC-1 solution for 10 minutes on an 80°C water bath. Silicon wafers were then rinsed with Milli-Q water and etched in a hydrofluoric acid/ammonium fluoride buffer solution for 2 minutes. The wafers were then rinsed again with Milli-Q water prior to being placed in a mixture of Milli-Q water, hydrogen peroxide, and hydrochloric acid in a 4:1:1 volume ratio for 10 minutes on an 80°C water bath. This mixture is known as the standard cleaning solution-2 (SC-2) solution. Following this step, hydroxyl-terminated Si (100) wafers are pulled for use as controls. To produce the hydrogen-terminated Si (100) wafers, the remaining samples are rinsed using Milli-Q water and etched a second time in the hydrofluoric acid/ammonium fluoride buffer solution for 1 minute. These freshly etched samples were then dipped in an ammonium fluoride solution for 6 minutes.

2.2 Preparation of chlorine-terminated Si(100) surfaces

To chlorinate the samples a procedure described in a paper by Bansal et al. was used [1]. Hydrogen-terminated Si-(100) wafers, prepared as described in Sec. 2.1, were rinsed in chlorobenzene before being placed in a solution of chlorobenzene and phosphorous pentachloride. Benzoyl peroxide was added to the solution to serve as a radical initiator. Prior to the start of the reaction, the PCl_5 solution was purged under nitrogen for 30 minutes to remove gaseous impurities. The reaction took place at 110°C for 1 hour on an oil bath.

2.3 Preparation of 4-fluorophenylboronic acid modified Si (100)

The termination of Si (100) with 4-fluorophenylboronic acid was described previously in a paper by Byron et al [2]. A 30 mM solution of 4-fluorophenylboronic acid was made, using toluene as a solvent. This was mixed for 1 hour at 100°C. Freshly chlorinated samples, prepared as described in Sec. 2.2, were then placed in the chlorinated solution for 3 hours at 50°C on an oil bath under nitrogen.

2.4 Atomic layer deposition of titania thin films on modified Si (100) surfaces

Prepared samples were placed in a commercial Oxford FlexAL II Thermal/Plasma ALD chamber in the UD Nanofabrication Facility. Each ALD cycle consisted of a 1 second dose of tetrakis(dimethylamido)titanium (TDMAT), 10 second Argon purge, 60 second vacuum pump down, 20 milliseconds of water, another 10 second Ar purge, and an additional 60 second pump down. Reactants were delivered via a 200 sccm argon carrier gas and purges were done using 100 sccm argon. The temperature in the ALD was kept constant at 130°C and the base pressure in the ALD reactor was 7×10^{-9} torr.

2.5 Characterization Techniques

2.5.1 X-ray Photoelectron Spectroscopy (XPS)

All XPS analysis was done on a Thermo Scientific K-Alpha+ using an Al Kα source ($h\nu$ = 1486.6 eV). The base pressure was 3.75× 10^{-9} torr with a takeoff angle of 35.3° with respect to the analyzer. All high-resolution spectra were taken with a pass energy of 20 eV, step size of 0.1 eV, and 50 millisecond dwell time. Spectral features were calibrated using the carbon 1s peak at 284.6 eV. Spectra were analyzed using CasaXPS (Version 2.3.26).

2.5.2 Atomic Force Microscopy (AFM)

AFM images were taken in tapping mode using an Anasys Nano IR2 system. All images were processed with GWYDDION software (version 2.66).

2.5.3 Time-of-flight secondary ion mass spectroscopy (ToF-SIMS)

The ToF-SIMS analysis was done on an IONTOF TOF.SIMS 5, using a 30 keV, 0.13 pA Bi^+ primary ion beam. Sputtering was done using 500 eV Cs ion source for negative spectra and 500eV O_2 ion source for positive spectra. Data was processed using IONTOF's SurfaceLab (Version 7.3) data analysis package. Sputtering rates were determined via profilometry (Sec. 2.5.4) and ellipsometry (Sec. 2.5.5).

2.5.4 Profilometry

Profilometry was done using a Bruker Dektak XT profilometer with a tip width of 5 microns, range of 6.5 microns, and 3 mg force. These were run on the hill and valleys setting. This was used in combination with ToF-SIMS to calculate a 500eV silicon sputter rate of 0.125 $\frac{\mathrm{nm}}{s}$.

2.5.5 Ellipsometry

Ellipsometry was done using a Woolam M-2000. Titania thickness was determined using a three-layer Cauchy model (film/native oxide/silicon). The native oxide was assumed to be 2 nanometers thick. This was used in combination with ToF-SIMS to calculate a 500eV titania sputter rate of 0.112 $\frac{\text{nm}}{s}$.

2.5.6 Scanning Electron Microscopy (SEM)

All SEM images were taken using an AURIGA 60 Crossbeam FIB-SEM.

2.6 Diffusion Modeling

Throughout the calculations for root mean squared diffusion, a one-dimensional planar Fickian diffusion model is used to determine the estimated spread of a particle in Brownian motion. The equation for the RMS diffusion in this one-dimensional case is given by the following equation.

$$x_{RMS} = \sqrt{2\int_0^t D(\tilde{t})\, d\tilde{t}} \quad \text{(Eq. 1)}$$

This equation simplifies in the case where the diffusion coefficient is constant to the following equation.

$$x_{RMS} = \sqrt{2Dt} \quad \text{(Eq. 2)}$$

Equation 2 was used to estimate potential heat loads for annealing to produce meaningful impact in diffusion. However, once temperature profiles were obtained from the annealing process, actual RMS diffusion was calculated within MATLAB by calculating the diffusion coefficient for each value of temperature and taking the trapezoidal integral over the timespan for which the diffusion coefficient Arrhenius expression found in Eq. 3 was valid [4].

$$\mathrm{D} = 2^{+40}_{-1.9}\,\frac{cm^2}{s} \times \mathrm{Exp}\left[-\frac{3.45 \pm 0.25\ \mathrm{eV}}{k_b T}\right] \quad (\mathrm{Eq.}\ 3)$$

Furthermore, due to the relationship between the standard deviation of a Gaussian concentration profile and the mean squared displacement the average value of the diffusion coefficient can be back-calculated as shown below in Eq. 4.

$$D = \frac{\sigma^2}{2t} \quad (\mathrm{Eq.}\ 4)$$

Chapter 3

Results and Discussion

3.1 Study of Boron Diffusion at Large Heat Loads in a Vacuum Tube Furnace

3.1.1 Methodology

Given that the annealing of this particular small molecule inhibitor has not yet been studied, the effects of large heat loads and diffusion were to this point unknown and were studied using a medium vacuum tube furnace ($\sim 10^{-3}$ torr). Hydroxyl-terminated Si(100) was prepared through the methods described in section 2.1. FPBA-terminated samples were also prepared through the sequence shown in section 2.4. These samples were analyzed in XPS to determine the surface coverage of FPBA using eq. 5[6].

$$\Phi_{OV} = \left(\frac{\lambda \sin(\theta)}{\mathrm{a_{Ov}}}\right)\left(\frac{SF_{Si}}{SF_{Ov}}\right)\left(\frac{\rho_{Si}}{\rho_{Ov}}\right)\left(\frac{I_{Ov}}{I_{Si}}\right) \quad (Eq. 5)$$

Where λ represents the penetration depth (2.0 nm in this instrument), θ represents the photoelectron takeoff angle (45°); I is the intensity of the high-resolution peak in XPS, a_{Ov} is the atomic diameter of the overlayer species, obtained through eq. 6 [6].

$$a_{Ov} = \left(\frac{A_{Ov}}{\rho_{Ov} N_A}\right)^{\frac{1}{3}} \quad (Eq. 6)$$

Where A_{Ov} is the atomic weight of the overlayer species and N_A is Avogadro's constant. For the given equations, a monolayer is defined as one boron atom per silicon atom. Since FPBA is a bidentate ligand, the surface coverage, as it has been

defined, can only reach a maximum of 50%. Three heat treatments were used to study the effects of diffusion as outlined in Table 1.

Table 1: Heat Treatments for Samples Annealed in the Tube Furnace

Sample	**Temperature (°C)**	**Time (min)**	**Estimated RMS Diffusion (nm)**
Control	---	---	---
1	850	15	10.9
2	850	30	15.4

3.1.2 Surface Characterization

3.1.2.1 X-Ray Photoelectron Microscopy

Prior to the deposition of titania, the surface coverage of FPBA was found using XPS. Using the ratio of fluorine and silicon intensities across three points, in combination with equations 5 and 6, the surface coverages of FPBA were found and can be viewed in table 2. Silicon intensity was found using a Shirley background and boron intensity was found using a linear background.

Table 2: Surface Coverage Calculations for Tube Furnace Samples

Point	Silicon Intensity (counts)	Boron Intensity (counts)	Surface Coverage (% Monolayer)
1	198022	2842	34.2
2	199566	2397	28.6
3	212784	2103	23.6
Average Surface Coverage (% Monolayer)		29 $\pm$ 5	

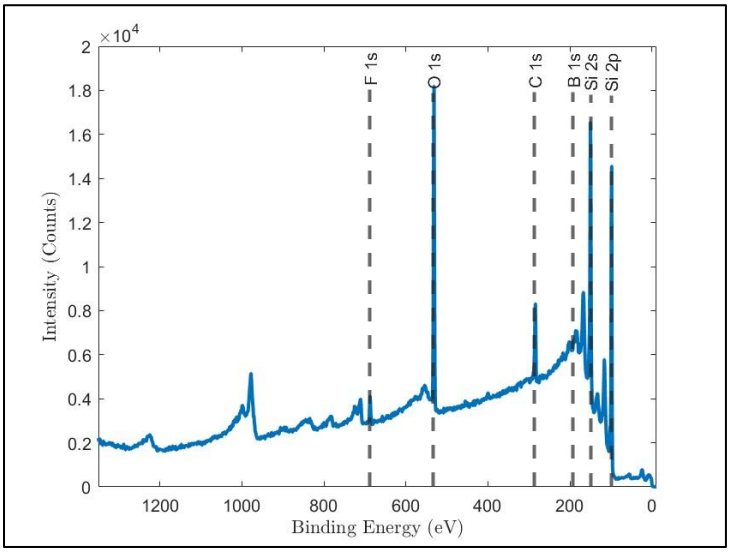

Figure 3: XPS Survey Spectrum from Tube Furnace Experiments

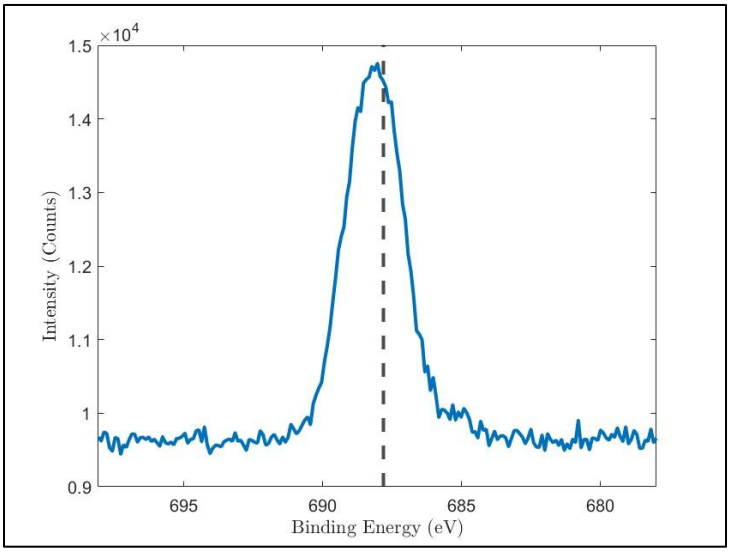

Figure 4: XPS High Resolution Fluorine 1s Spectrum from Tube Furnace Experiments

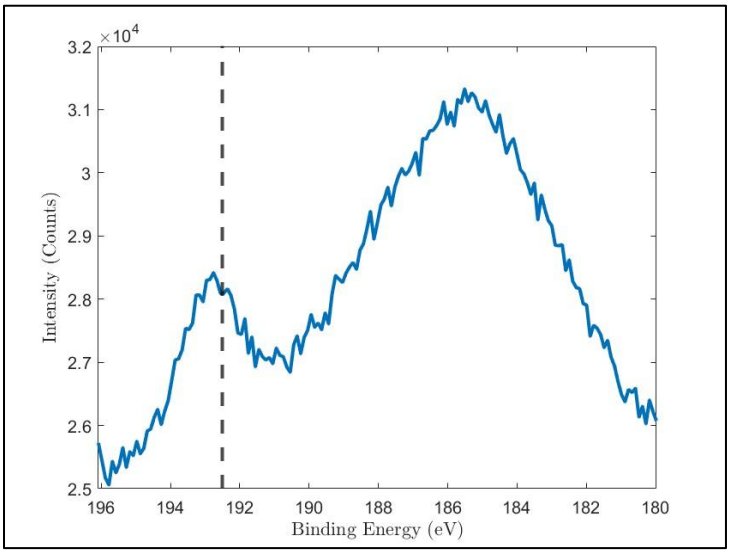

Figure 5: XPS High Resolution Boron 1s Spectrum from Tube Furnace Experiments

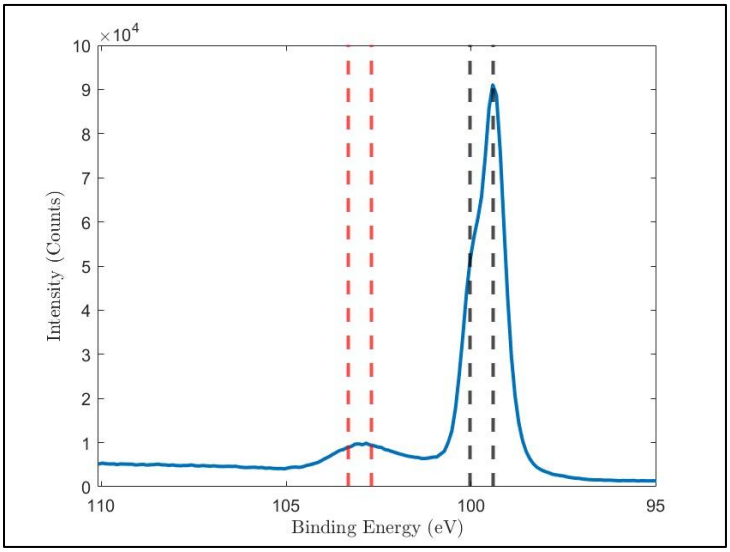

Figure 6 XPS High Resolution Silicon 2p Spectrum from Tube Furnace Experiments

The obtained XPS spectra were consistent with FPBA modification of the silicon surface. Present on the boron 1s spectra, is the silicon 2s plasmon loss peak. The red dashed lines in figure 6 represent the oxide peak of the silicon 2p spectrum. The black lines indicated the positions of the spin-orbit coupled 2p lines for crystalline silicon.

3.1.2.2 Atomic Force Microscopy

After the samples were annealed, they were moved to AFM to ensure the surface did not exhibit enough surface damage to convolute ToF-SIMS measurements. The images can be found below in figures 7 and 8.

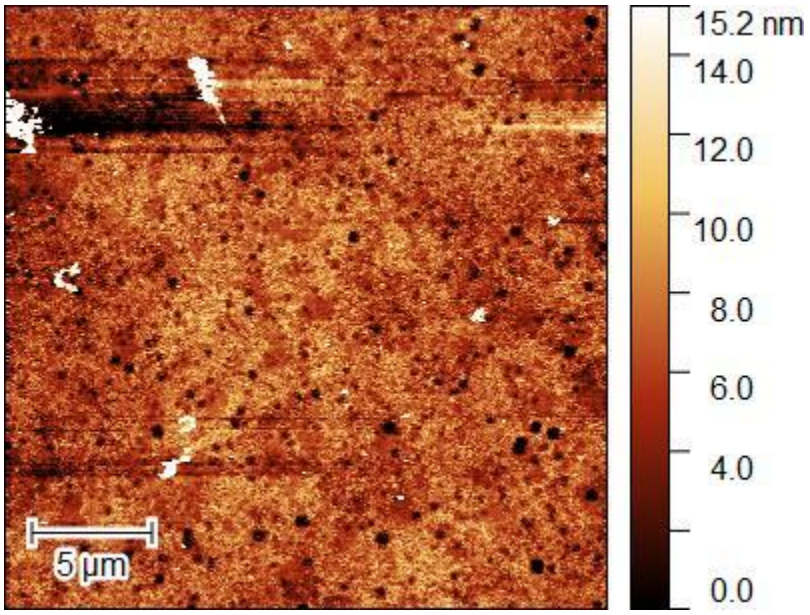

Figure 7: 15 Minute Tube Furnace Anneal AFM Image

The surface in Figure 7 shows signs of etch pit formation which may complicate the interpretation of the results of the ToF-SIMS. To verify this, the image was processed within Fiji and the threshold value set to identify the etch pits. The total area of the etch pits was then found to be 7.4% of the total area of the image. While this may produce some confounding effects, the number is small enough to still provide valuable information.

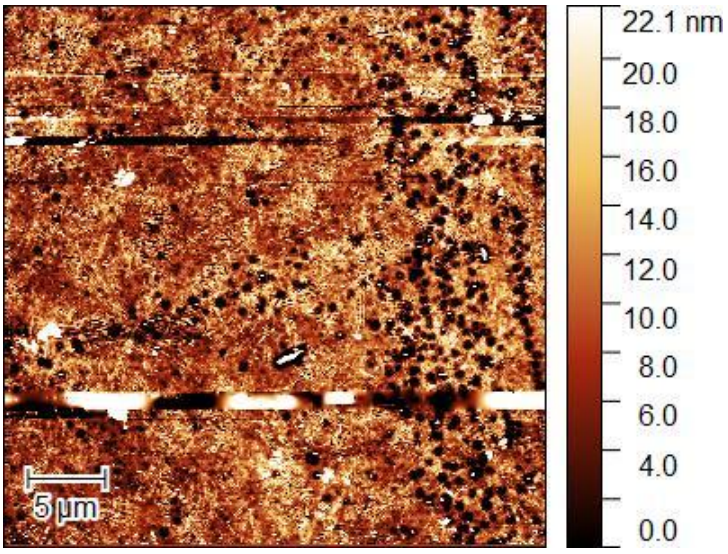

Figure 8: 30 Minute Tube Furnace Anneal AFM Image

The surface of the 30-minute samples in Figure 8 suffers from significantly more etch pits taking up significantly more of the area of the sample. A similar analysis in Fiji shows that the etch pits now take up 24.1% of the sampled area of the surface, significantly convoluting the data and likely calls the data's viability into question. For this reason, while the 30-minute anneal data will be present in future analysis, it is important to keep in mind this limitation.

3.1.2.3 SEM Images

The SEM images confirm the presence of surface damage observed by AFM. These images can be found below in figure 9 and 10. The damage in the 30-minute sample is, again, much more extensive than that of the 15-minute sample and cracks appear on a larger scale.

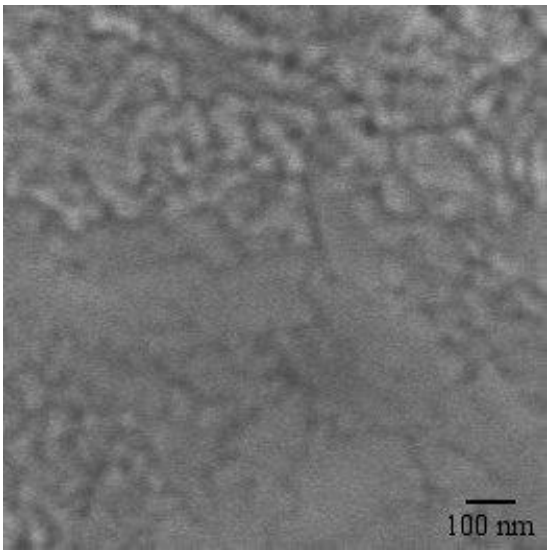

Figure 9: 15 Minute Tube Furnace Anneal SEM Image

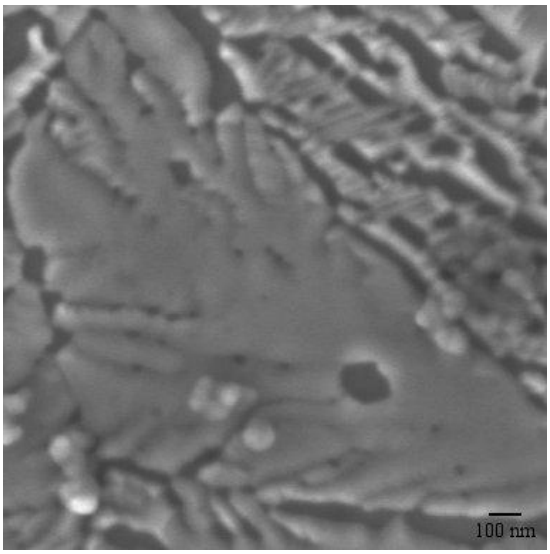

Figure 10: 30 Minute Tube Furnace Anneal SEM Image

This damage can clearly affect the ToF-SIMS investigation presented below, which is why the 15-minute annealed sample will be the primary sample analyzed.

3.1.3 Depth Profiles

3.1.3.1 Silicon and Titania Interdiffusion

Layered samples, which have been annealed for extended periods of time, will have some degree of interdiffusion via a substitution mediated mechanism. The effect of this interdiffusion was investigated using a hydroxyl-terminated silicon sample given an identical treatment as that of the FPBA-terminated sample. The Si_3^- fragment was used for silicon as it is a good representation of the bulk of silicon and does not show up in high enough quantities to saturate the detector. For similar reasons the TiO^- fragment was chosen to analyze the titania layer. The depth profiles can be found below in figure 11.

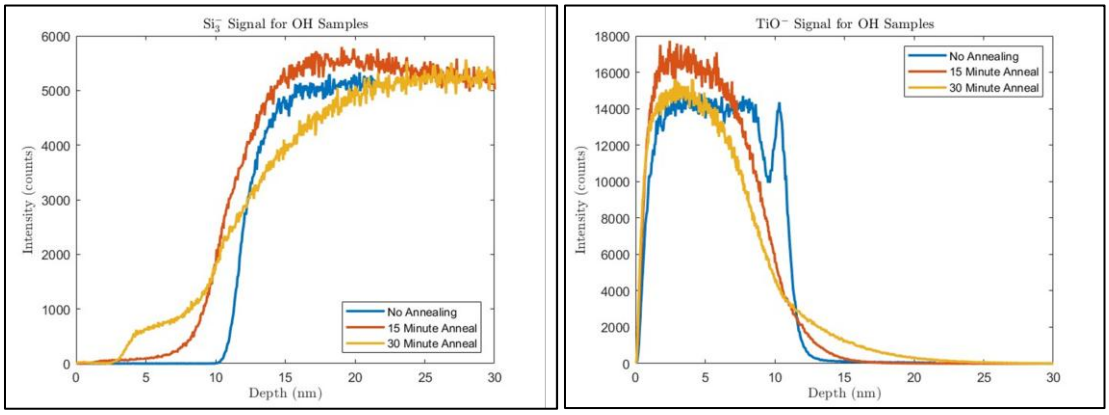

Figure 11: Si_3^- and TiO^- Fragments in ToF-SIMS

The once prominent dip in titania signal, likely resulting from a decreased density film at the initial stages of ALD, is eliminated post-anneal as the atoms can rearrange themselves easier given the additional energy. Broadening of the interface is evident in both the silicon signal and the titania signal as well, with longer anneals having a

slower drop off resulting from interdiffusion. As expected from the AFM and SEM data, the 30-minute anneal sample shows a complex depth profile complicated by the cracks developed in the sample, as evidenced by the sharp rise of the Si_3^- signal around 3 nm depth.

3.1.3.2 Fluorine Diffusion

Fluorine has been shown in previous work to diffuse out of titania layers given the much larger diffusion coefficient in titania (10^{-8} [3]) than silica (10^{-15} [9]). This trend holds true for these samples. The depth profile for fluorine across the samples can be found below in Figure 12.

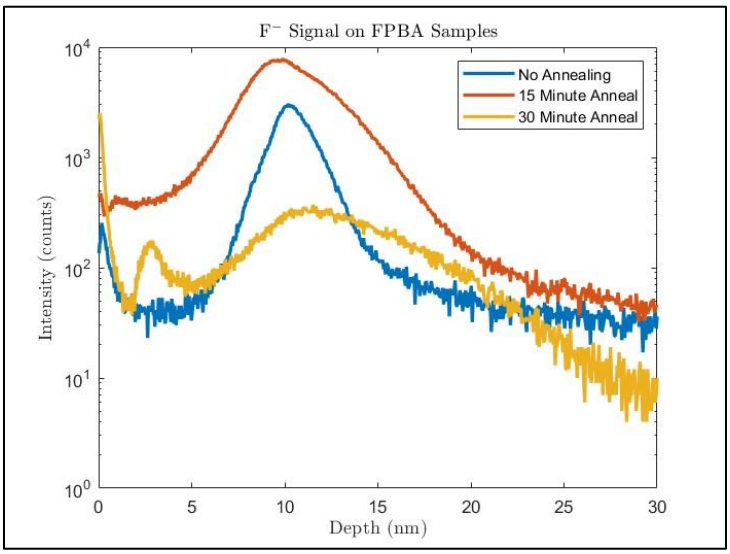

Figure 12: Depth Profiles of the F^- fragment in ToF-SIMS Tube Furnace Samples

The diffusion of fluorine can be clearly observed by comparing the sample without annealing and the 15-minute anneal visible via a broadening of the depth profile.

There does seem to be a higher concentration of fluorine located on the titania side of the interface (left) rather than the silicon side of the interface. While this may have to do with the surface damage allowing for fluorine to be detected earlier in the depth profile, literature also suggests that fluorine should diffuse faster into titania than silicon [13].

3.1.3.3 Boron Diffusion

Boron diffusion is the most important factor when determining the efficacy of using FPBA to selectively dope substrates. However, due to boron's relatively low detectability in ToF-SIMS, with our only being able to detect concentrations up to $1 \times 10^{18} \frac{\text{counts}}{\text{cm}^3}$, longer anneals with larger diffusion presents difficulties in detectability. However, a small yet noticeable boron signal was detected in ToF-SIMS. The signal was plotted on both a linear and semilogarithmic basis, as shown in Figure 13. Note, the boron signal for the 15-minute anneal was multiplied by 30 to provide easier comparison in the profiles.

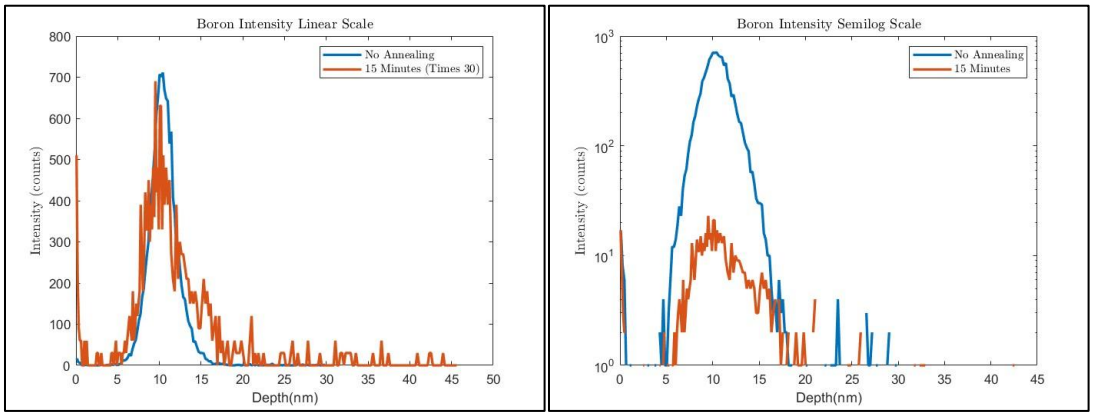

Figure 13: Linear and Logarithmic Boron Signals for Tube Furnace Samples in ToF-SIMS

The boron profiles have a noticeable asymmetry towards the underlying silicon layer, suggesting that the boron does preferentially diffuse into the silicon. This is promising especially considering that surface damage, resulting in earlier detection of fragments, would provide a shift towards the surface of the sample rather than the substrate. To better understand the differences in the profile, a Gaussian curve was fitted to the profiles on both the titania-side and silicon-side of the interface. The interface position was determined to be at the peak boron intensity and the peak of the Gaussian was fixed at the position of the interface. Below in Figure 14 and 15 the peaks can be found, normalized to a maximum intensity of one, and the fitted parameters for the Gaussians can be found in Table 3. Depth is measured as distance from the interface.

Table 3: Boron Gaussian Curve Fits for Silicon Side Tube Furnace Samples

Sample	**Fitted Side**	**A**	**B**	**C**	**Adjusted R^2**
Control	Silicon	660 ± 20	10.01	2.04 ± 0.07	0.987
Control	Titania	640 ± 20	10.01	1.77 ± 0.06	0.991
15 Minute	Silicon	13.4 ± 0.8	10.01	5.0 ± 0.4	0.871
15 Minute	Titania	16 ± 1	10.01	2.4 ± 0.3	0.894

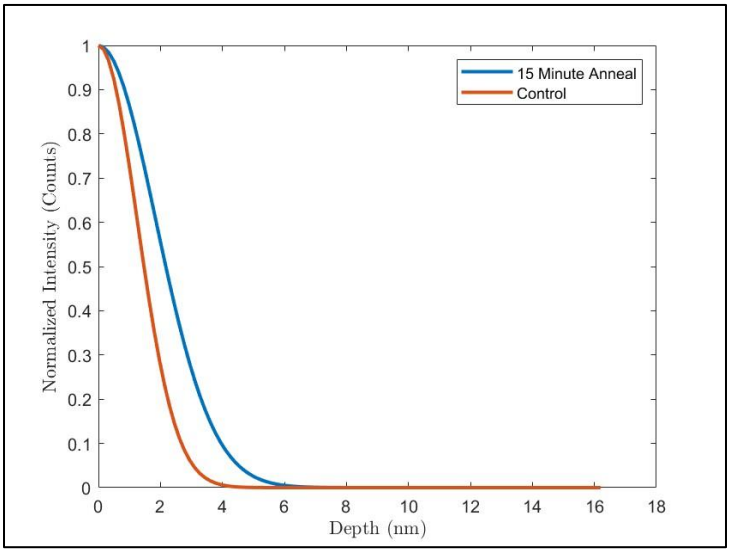

Figure 14: Titania Side Gaussian Curve Fits Tube Furnace Samples

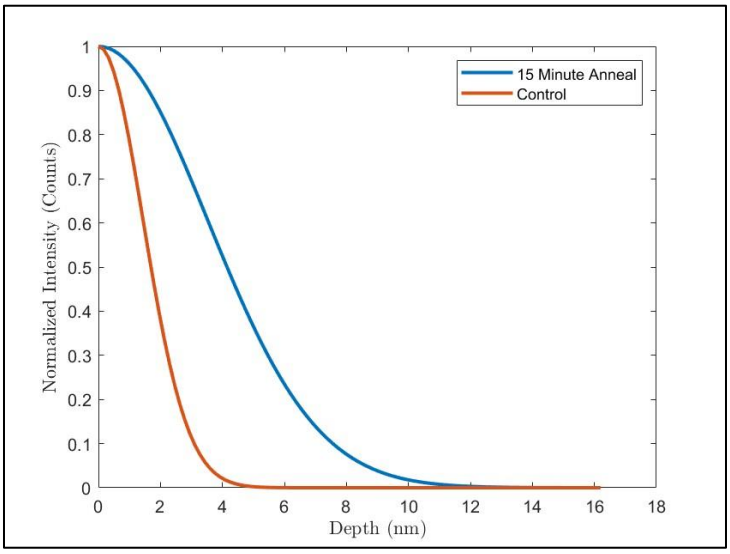

Figure 15: Silicon Side Gaussian Curve Fits Tube Furnace Samples

The figures demonstrate little diffusion in the titania side of the curve fit compared to the significant diffusion seen for silicon in the 15-minute sample. This confirms the

hypothesis that not only will boron diffuse into silicon preferentially, but it can also do so efficiently, making the approach practical.

3.2 Study of Diffusion Using Rapid Thermal Annealing

While the high heat load diffusion was studied using a conventional vacuum tube furnace, this is not how processing is performed in the modern day. Now, rapid thermal annealing (RTA) is used to drive dopants into the substrate and activate them without causing significant crystallographic changes due to the short annealing time. For this reason, another set of samples were prepared to study any differences, which may come from the new method of annealing.

3.2.1 Methodology

Four FPBA samples with 200 cycles of TDMAT-Water ALD were prepared as discussed in section 2.3 and section 2.4. The breakdown of the sample along with the heat treatments can be found below in Table 4.

Table 4: First Rapid Thermal Annealing Samples Heat Treatments

Sample	**Temperature (°C)**	**Time Above 600°C (sec)**	**Estimated RMS Diffusion (nm)**
Control	0	0	0
1	875	14.1	1.29
2	875	28.3	3.50
3	950	27.2	12.97

Note, the temperatures and times are considered estimates. The temperature profiles of the annealing can be found below in figure 16. Due to the fact that no flash drives are allowed in the cleanroom, the temperature profiles themselves could not be recovered at the time of these experiments and as such document scans were taken and later sent into an online image processor to produce the temperature as a function of time. Using this data the temperature was converted to a diffusion coefficient using the techniques shown in section 2.6.

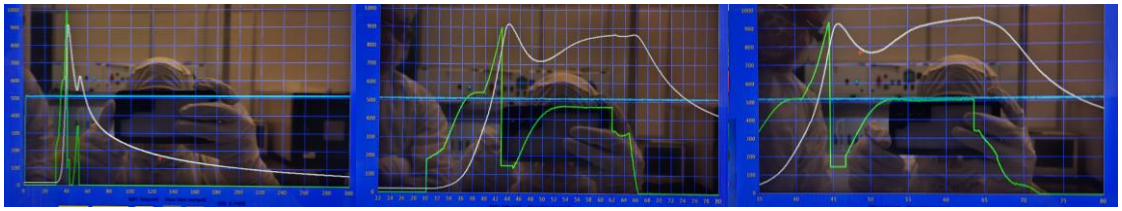

Figure 16: First RTA Experiment Temperature Profiles (Samples in order 1-3)

The temperature profile is represented by the white line within the photographs. Again, due to the inability to use a flash drive within the cleanroom, these were the best images available. The temperature profiles were not well controlled, which likely lead to increased surface damage due to thermal expansion and hot spots forming. In addition, due to the samples being very thin films there was likely some crystallization in the samples, which would cause changes in density and cracking. This claim was tested using a bench top XRD instrument, but the only visible peaks were those of the Si(100) substrate.

3.2.2 Surface Characterization

3.2.2.1 X-ray photoelectron spectroscopy

Using equations 5 and 6, the surface coverages of FPBA were determined yet again. The results of these surface coverages can be found below in table 5.

Table 5: XPS Surface Coverage for First RTA Samples

Point	Silicon Intensity (counts)	Boron Intensity (counts)	Surface Coverage (% Monolayer)
1	178430	6054	32.3
2	190705	5220	26.1
3	198433	3950	19.1
Average Surface Coverage (% Monolayer)		26 ± 7	

The sample survey spectrum for the FPBA samples used to calculate these surface coverages can be found below in figure 17, and the high-resolution spectra for fluorine, boron, and silicon can be found in figure 18, 19, and 20 respectively.

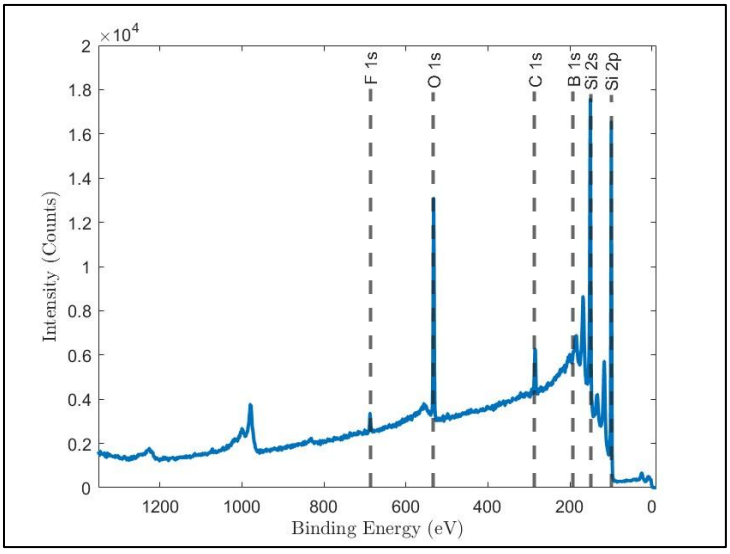

Figure 17: Survey spectrum for first rapid thermal annealing experiment

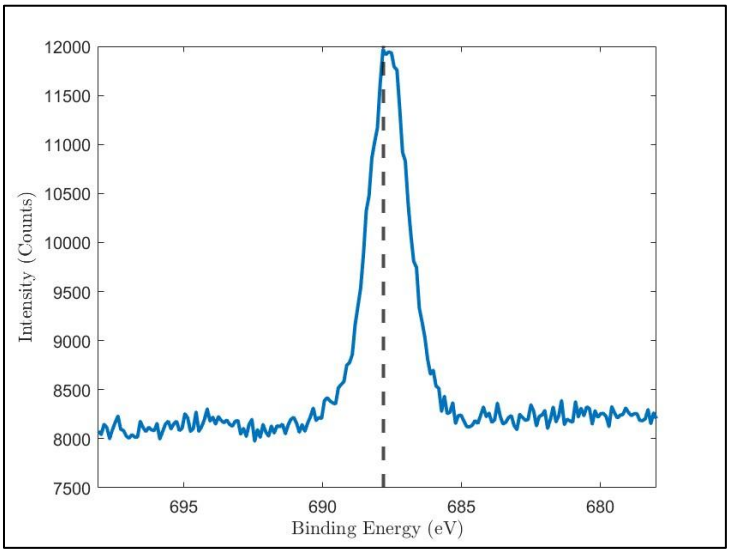

Figure 18: XPS High Resolution Fluorine 1s Spectrum from First RTA Experiments

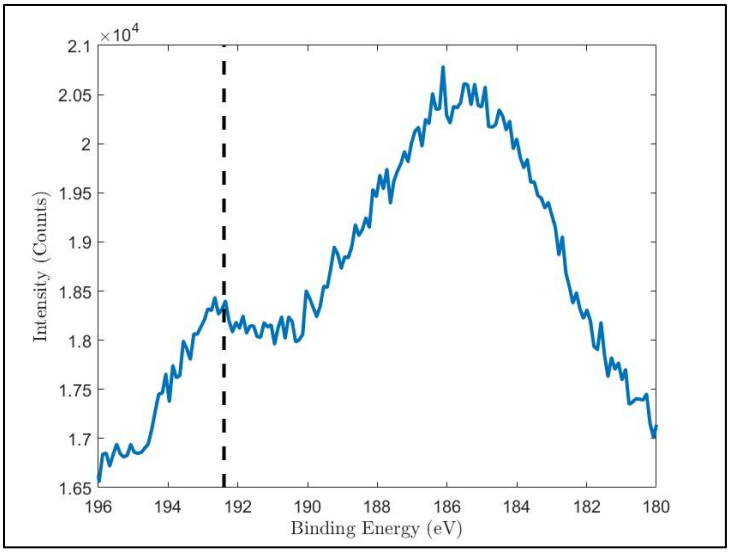

Figure 19: XPS High Resolution Boron 1s Spectrum from First RTA Experiments

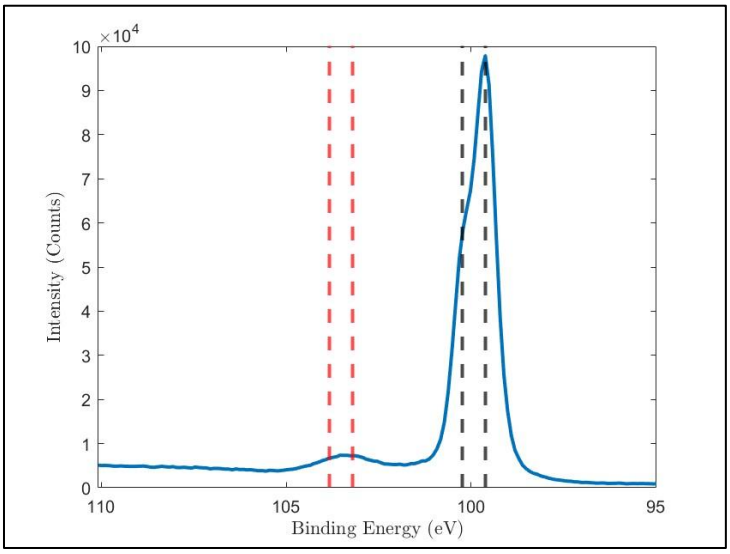

Figure 20: XPS High Resolution Silicon 2p Spectrum from First RTA Experiments

These surface coverages are comparable to the first set of samples and were high enough to continue with the annealing. Just like in the previous set of experiments, nothing unexpected was observed in XPS.

3.2.2.2 Atomic force microscopy

After the annealing, AFM was performed and analyzed in Gwyddion and Fiji to determine the degree of surface damage. Images for the annealed samples can be found in figure 21, 22, 23, and 24 for the control, sample 1, sample 2, and sample 3, respectively.

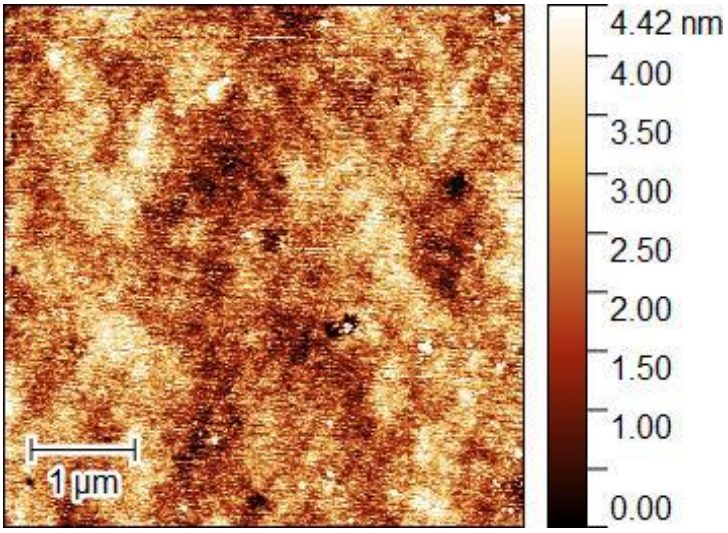

Figure 21: AFM Data for First RTA Experiment Control Sample

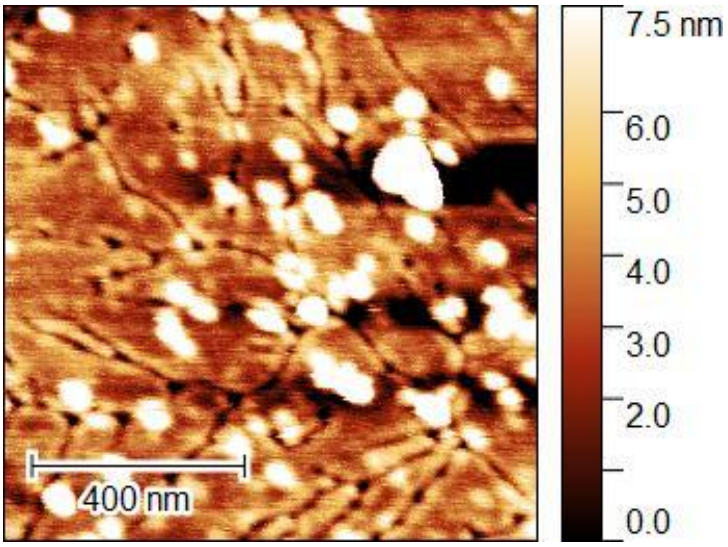

Figure 22: AFM Data for Sample 1

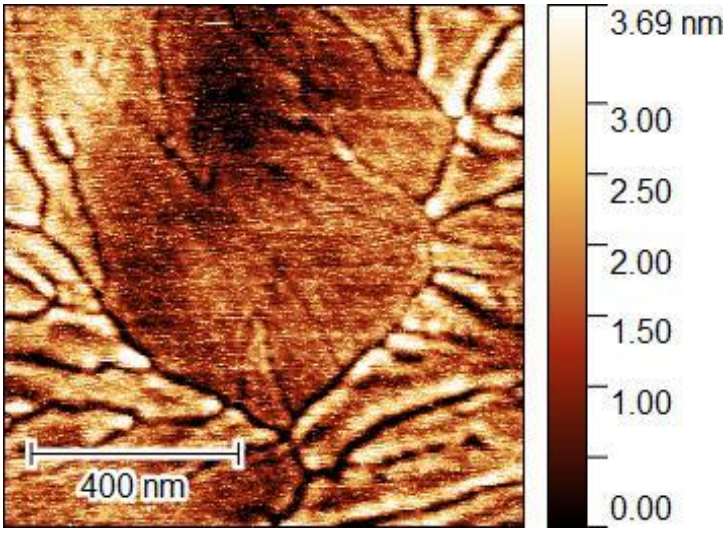

Figure 23: AFM Data for Sample 2

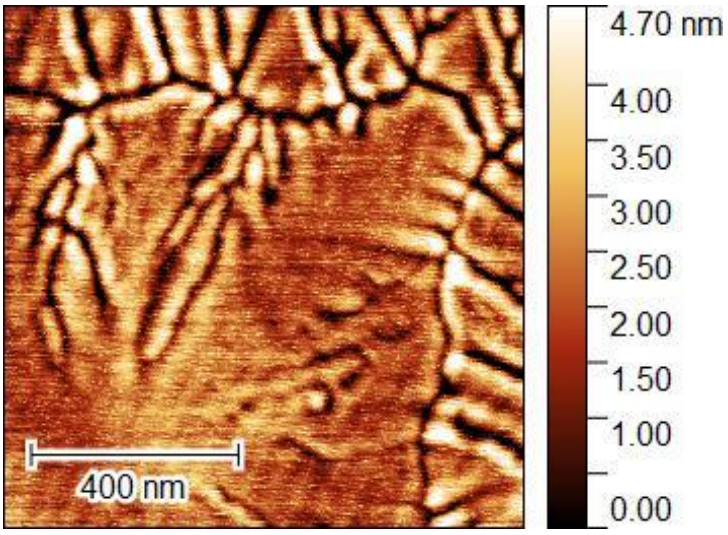

Figure 24: AFM Data for Sample 3

Although the samples saw noticeable damage in the tube furnace with the sample 1,2, and 3 receiving numerous cracks adding up to roughly 10%, 16%, and 18% of the surface as verified in Fiji, the damage is confined to the topmost few nanometers of the samples. Although this may complicate the results of ToF-SIMS investigation below, this damage is certainly much less pronounced than that for the 30 minute anneal sample described above (where the cracks extended up to 20 nm in height).

Depth Profiles

3.2.2.3 Boron Depth Profiles

The boron depth profiles show damage at the surface of samples 2 and 3 with flat depth profiles for boron. This is likely because the Boron at the interface could be immediately detected. This is shown below in Figure 25.

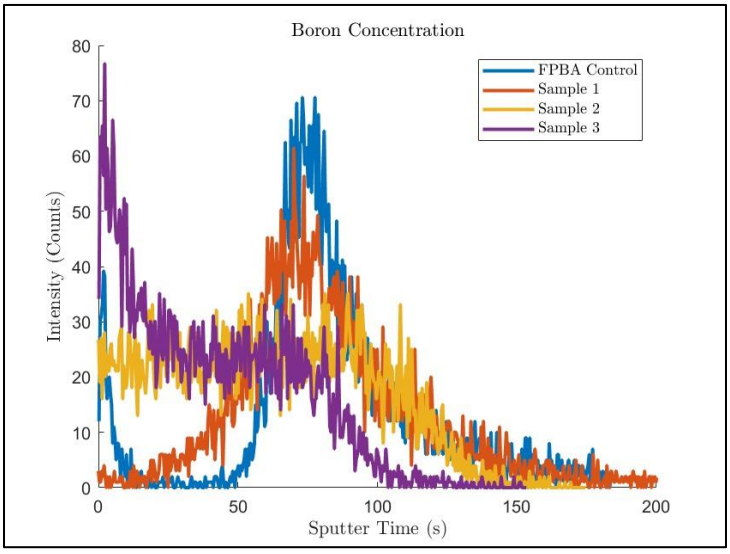

Figure 25: ToF-SIMS Depth Profile of Signal vs Sputter Time for First RTA Samples

For clarity, the sample 2 and 3 spectra will be omitted moving forward. The remaining samples were then depth calibrated and are shown below in Figure 26.

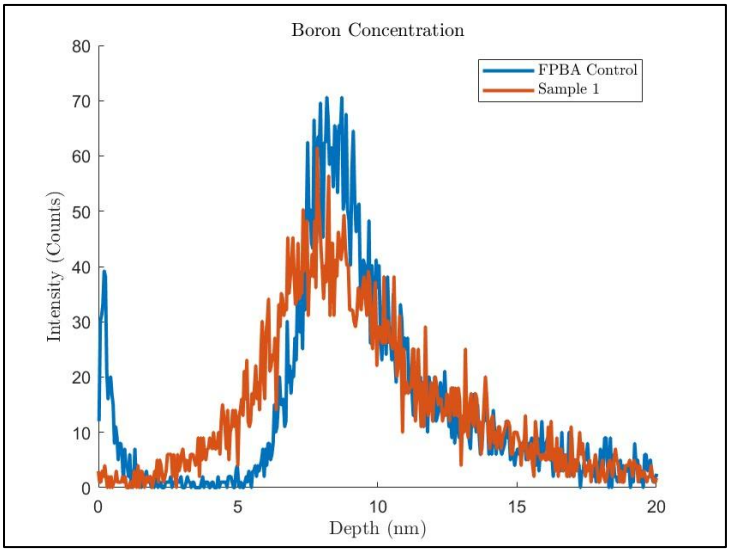

Figure 26: ToF-SIMS Boron Depth Profile of the Control and Sample 1

The peak boron intensity, as expected, decreased between the control and annealed sample. This makes the diffusion visually less noticeable into silicon (Depth > 8.2 nm). For this reason, like the tube furnace samples, Gaussian curve fits were made with respect to both sides of the interface. The fitting parameters can be found below in Table 6. The curve fits, normalized to a maximum intensity of 1 to better visualize the change in the distribution of boron, can be found below in figure 27 and 28 for the silicon side and titania side curve fits respectively.

Table 6: Gaussian Curve Fit Parameters for the Control Sample and Sample 1

Sample	**Fitted Side**	**A**	**B**	**C**	**Adjusted R^2**
Control	Silicon	$50. \pm 2$	8.20	3.3 ± 0.2	0.845
Control	Titania	60 ± 2	8.20	1.33 ± 0.06	0.953
Sample 1	Silicon	38 ± 1	8.20	5.2 ± 0.2	0.894
Sample 1	Titania	$40. \pm 2$	8.20	2.8 ± 0.1	0.921

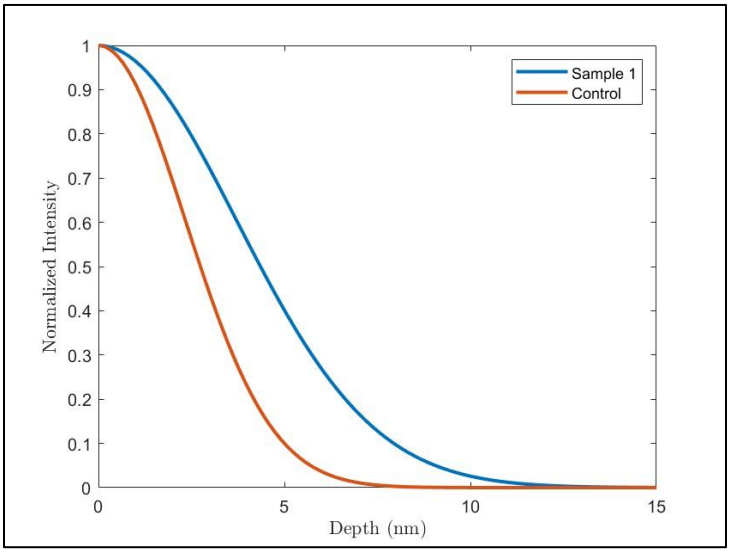

Figure 27: Silicon Boron Distribution Gaussian Curve Fit Normalized to Maximum Intensity of Unity

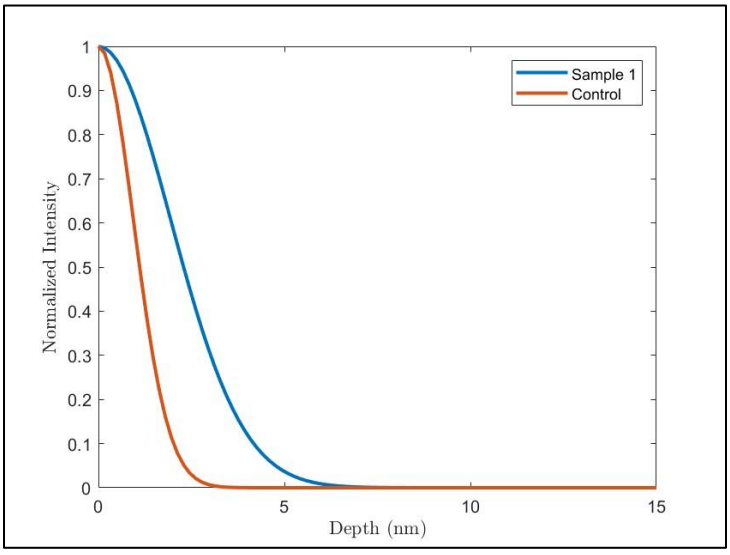

Figure 28: Titania Boron Distribution Gaussian Curve Fit Normalized to Maximum Intensity of Unity

The preferential diffusion into silicon can again be shown above. Of note is the difference between standard deviations of sample 1 and the control. This difference can be used to find the average change in the RMS displacement due to annealing. Using Eq. 3 from earlier, again assuming a planar dopant profile with 1-D diffusion, the diffusion coefficient can be back-calculated and compared with literature values to evaluate the model's accuracy. The difference between the standard deviations for the silicon side was $1.9\ \text{nm} \pm 0.4\ \text{nm}$. For the region of interest, the amount of time at which the sample was above 600°C was used, as below this temperature there is not a significant amount of diffusion occurring. This was plugged into Eq. 3 to produce a diffusion coefficient of $1.3^{+0.6}_{-0.5} \times 10^{-15}\ \frac{\text{cm}^2}{\text{s}}$. This is remarkably close to the value of the diffusion coefficient according to the Arrhenius relationship modeled by Cowern et al. [4], which when calculated at the average temperature over the timespan generates a value of $1.44 \times 10^{-15}\ \frac{\text{cm}^2}{\text{s}}$.

3.2.2.4 Fluorine Depth Profile

In addition to the boron, the fluorine spectra were also analyzed. The size of the fluorine peak was greatly diminished, likely from so much fluorine diffusing out of the titania layer during annealing, that it dropped much of the concentration profile below the detectability limits within ToF-SIMS. Below in figure 29, is the fluorine profile on a linear scale, with the boron intensity for the annealed sample 1 multiplied by 20 to better visualize differences.

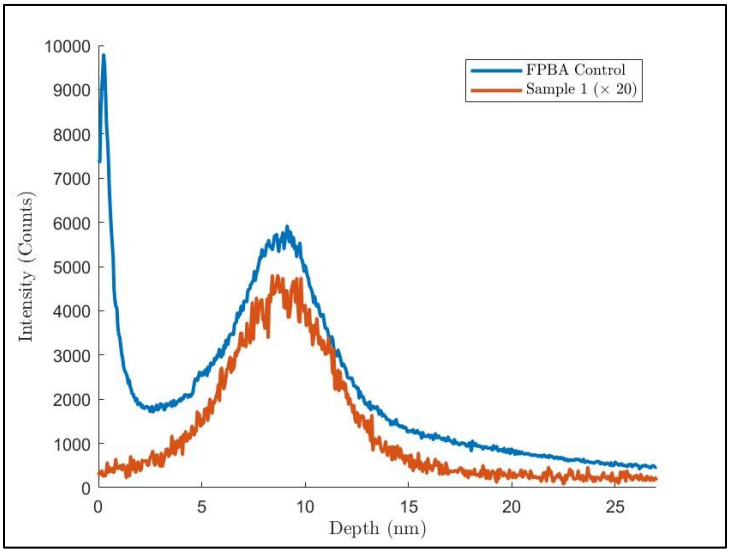

Figure 29: Fluorine Depth Profile for the Control Sample and Sample 1

The profile shows a slight broadening in both directions however, given how low the signal was and how much it dropped off. The true shape of the fluorine concentration profile may be very different from what is depicted above. Given that fluorine has a very high sensitivity in negative ToF-SIMS scans it is likely the concentration is very low.

3.3 Continued Rapid Thermal Annealing with Varied Heat Loads

3.3.1 Methodology

Given the extensive surface damage viewed in previous experiments, a more controlled thermal treatment was desired. Also, another set of experiments was performed on hydroxyl terminated silicon wafers with 200 cycles of TDMAT/H_2O ALD to determine which temperatures exhibited the least amount of damage. The tested temperatures were no annealing, 775°C, 800°C, and 850°C. The 850°C sample

was far too damaged to provide useful information, however, the remaining samples are shown below in Figure 30. The method of heating was also changed, with the sample being allowed to rest at 600°C for 1 minute before being lifted to the target temperature for 15 seconds.

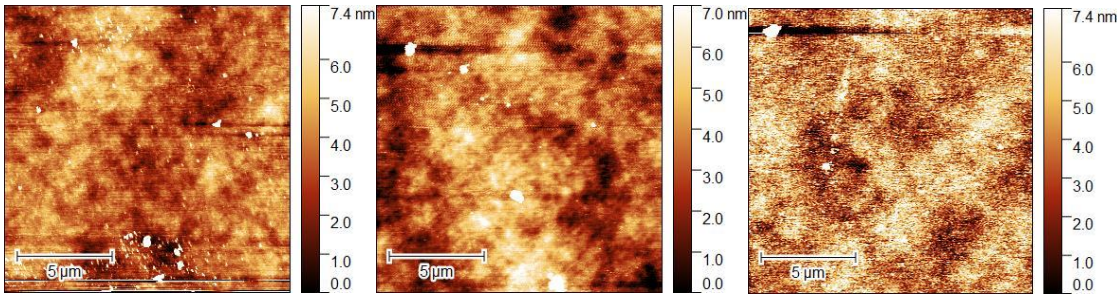

Figure 30: Heat Load Calibration Samples AFM (Control, 775°C Anneal, 800°C Anneal)

Given the minimal damage on the 775°C sample, it was decided to anneal the next set of samples to 750°C and vary the amount of time spent at that temperature. The sample numbers and their corresponding heat treatments can be found below in Table 6. In addition, a plot of the temperature profiles of the samples within RTA can be found in figure 31.

Table 6: Second RTA Annealing Experiment Sample Treatments

Sample	Temperature (°C)	Time Above 600°C (sec)	Estimated RMS Diffusion (nm)
Control	0	0	0
1	750	10	0.199
2	750	15	0.252
3	750	20	0.293

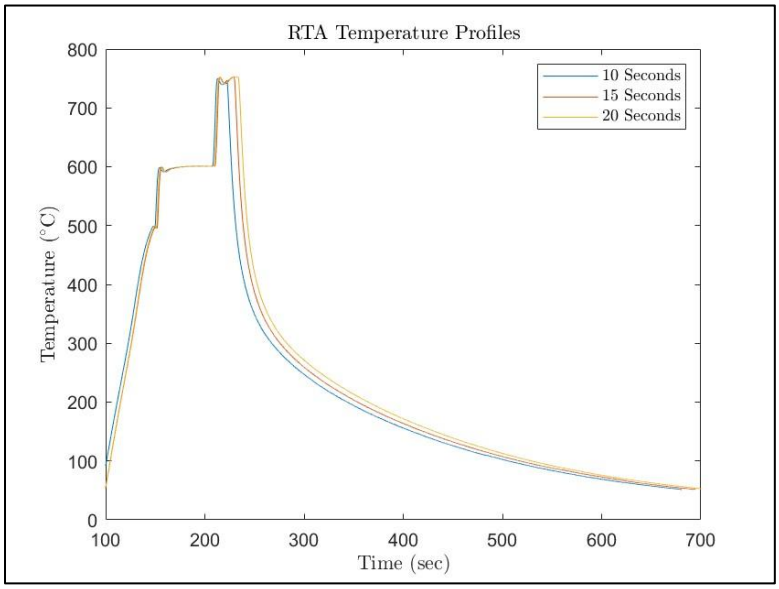

Figure 31: Temperature Profiles of the Second RTA Experiments

This set of samples were controlled much better than previous samples due to a better understanding of PID controllers.

3.3.2 Surface Characterization

3.3.2.1 XPS Spectra

As with previous samples, an XPS spectrum was taken to confirm the presence of FPBA on the surface and evaluate coverage. The results for the surface coverage of the samples can be found in table 7.

Table 7: FPBA Surface Coverage for Second RTA Experiment

Point	Silicon Intensity (counts)	Boron Intensity (counts)	Surface Coverage (% Monolayer)
1	355806	5284	35
2	343368	6532	45
3	331556	2256	16
Average Surface Coverage (% Monolayer)		30 $\pm$ 20	

Included with Table 7, is the survey spectrum, as shown in figure 32, and the high resolution spectra for fluorine (figure. 33), boron (figure. 34), and silicon (figure. 35).

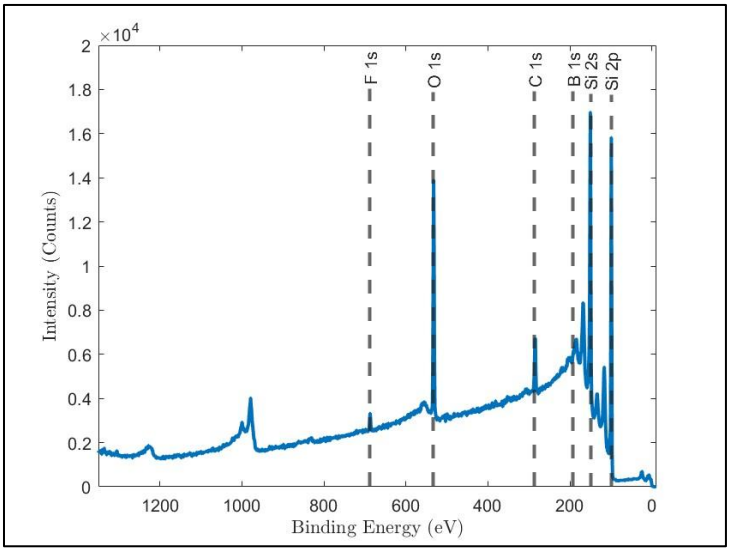

Figure 32: XPS Survey Spectrum of Second RTA Experiment FPBA Sample

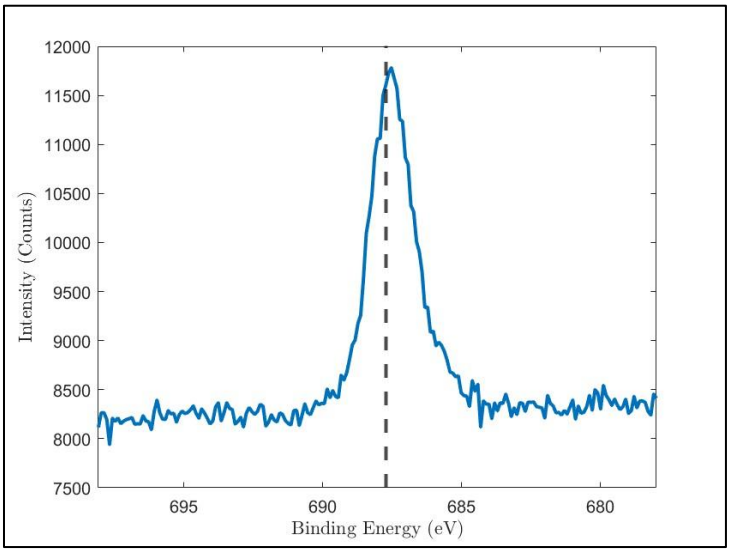

Figure 33: XPS High Resolution Spectra of Fluorine 1s for Second RTA Experiment FPBA Sample

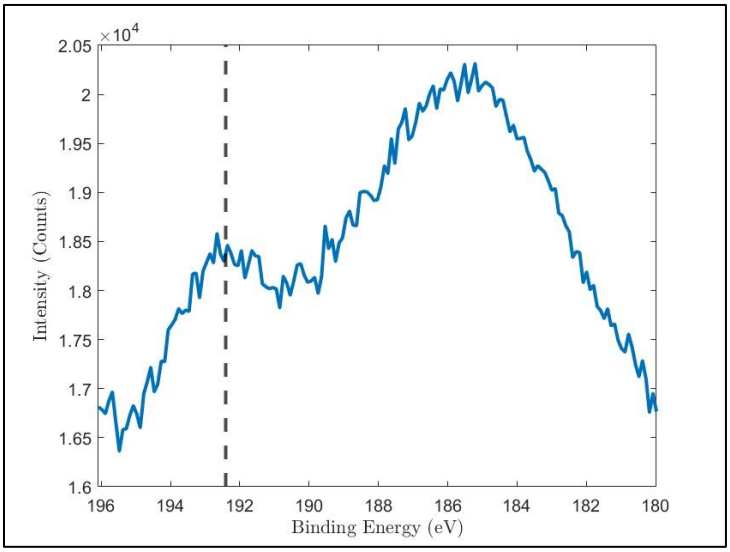

Figure 34: XPS High Resolution Spectra of Boron 1s for Second RTA Experiment FPBA Sample

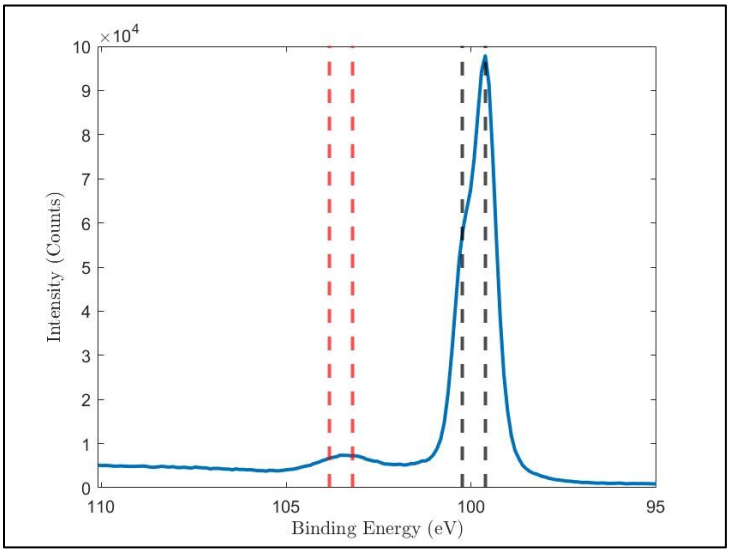

Figure 35: XPS High Resolution Spectra of Silicon 2p for Second RTA Experiment FPBA Sample

The surface coverage of the sample is reasonably high to continue with the annealing and the survey spectra revealed little to no impurities. However, the large standard deviation of different analysis points for the sample is worrying and may indicate nonuniform coverage. This would call into question some previously made assumption including 1-dimensional Fickian diffusion, as well as certain spots in ToF-SIMS receiving a higher boron concentration than others. However, the ToF-SIMS analysis area is sufficiently high (50 μm) to alleviate at least some of these concerns.

3.3.2.2 Atomic Force Microscopy

Following the ALD and annealing, the AFM of the FPBA samples were then taken. Unfortunately, some of the images were corrupted and are not available. However, the control sample and sample 3 still have intact images, and can be viewed below in figure 36.

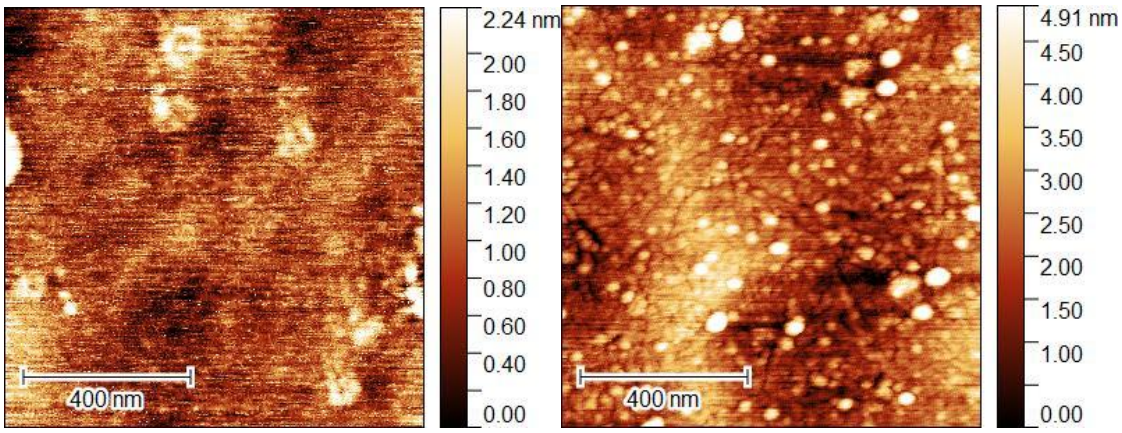

Figure 36: AFM of the control sample (left) and sample 3 (right) for the Second RTA Experiment

The sample after annealing shows remarkably little damage, with an RMS-roughness of 958 pm. Allowing for a non-convoluted depth-profile using ToF-SIMS. However, there are signs of initial damage on the surface with shallow cracking presenting itself. This additional damage may be due to volatile titanium fluoride species rapidly evaporating during the annealing, and it may be worthwhile studying this same procedure with phenylboronic acid, forgoing the fluorine.

3.3.3 Depth Profiles

3.3.3.1 Boron Depth Profiles

The boron depth profiles were taken after the annealing. The plots are shown below in figure 37.

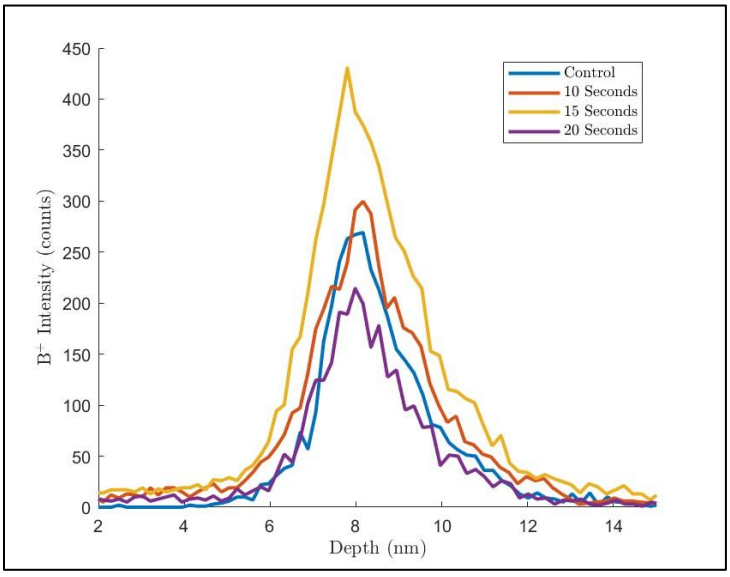

Figure 37: Boron Depth Profile for Second RTA Experiment

The signal intensities of the spectra vary significantly between different heat treatments. This may be an artifact of the nonuniform dopant distribution present on the surface. The 15 second anneal, for example, could have been taken in a location with a relatively high concentration of boron pushing into 40% of a monolayer. The control may have also been taken in a location with a lower boron concentration. Fitting Gaussian curves to the data in the manner described previously, the following plot was obtained and the best fit data tabulated in Table 8.

Table 8: Boron Gaussian Curve Fitting Parameters for Second RTA Experiments

Sample		**A**	**B**	**C**	**Adjusted R^2**
Control	Silicon	220 ± 10	8.17	1.8 ± 0.1	0.967
10 Seconds	Silicon	250 ± 10	8.17	2.1 ± 0.1	0.968
15 Seconds	Silicon	340 ± 20	8.17	2.2 ± 0.1	0.973
20 Seconds	Silicon	186 ± 8	8.17	2.0 ± 0.1	0.968

These parameters not only show the spreading of the data but also the changes in boron intensity at the interface with a nearly two-fold difference in the Gaussian peak across the 15-20 second anneal.

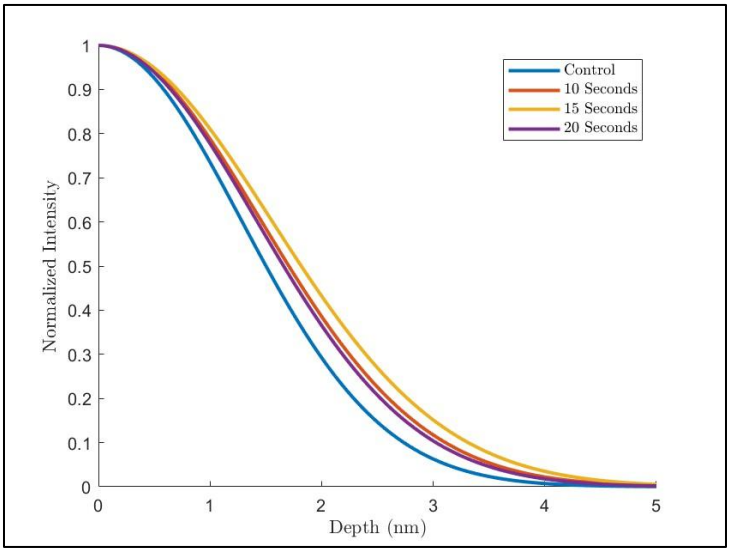

Figure 38: Gaussian Curve Fits for Boron Diffusion into Silicon for Second RTA Experiment

The visualization of the data seen in Figure 38 shows an increase in diffusion across all of the curves aside from the 20 second anneal. However, the differences are so small between the curves that it is difficult to decide with any certainty if there was any significant amount of diffusion. The difference in standard deviation between each sample and the control can be viewed in Table 9, along with the projected RMS diffusion for that heat load as acquired by trapezoidal integration of the temperature profile.

Table 9: Standard Deviation of Second RTA Samples Compared to RMS Displacement

Sample	**Change in Standard Deviation (nm)**	**Integrated RMS Displacement (nm)**	**Calculated Diffusion Coefficient** $(\frac{\mathbf{cm^2}}{\mathbf{s}})$	**Literature Diffusion Coefficient** $(\frac{\mathbf{cm^2}}{\mathbf{s}})$
10 Second Anneal	0.3 ± 0.2	0.199	$3.0^{+10.}_{-0.01} \times 10^{-17}$	2.03×10^{-17}
15 Second Anneal	0.4 ± 0.2	0.252	$4.8^{+10}_{-1.0} \times 10^{-17}$	
20 Second Anneal	0.2 ± 0.2	0.293	$9.0^{+40}_{-0.4} \times 10^{-18}$	

The data shows that the thermal loads may have been far too light to observe any real degree of diffusion across the samples. Especially since all samples, except for the 15 second sample, do not show a statistically significant change in the standard deviation of the Gaussian fit between themselves and the control. Also, the calculated diffusion coefficients, while at the same order of magnitude as the literature value for the diffusion coefficient, are consistently overestimating the value of the diffusion coefficient aside from the 20 second anneal, which agreed with at 95% confidence.

Chapter 4

Conclusion

This work demonstrates the feasibility of using small molecule inhibitors, specifically 4-fluorophenylboronic acid (FPBA), to direct dopant diffusion through selective surface functionalization and post-deposition annealing. By using AS-ALD deposited thin films with the SMI containing dopant enables controlled delivery of dopant to a buried interface. Using ToF-SIMS, dopant profiles were created and modeled using basic 1-dimensional Fickian transport theory. These measurements showed preferential diffusion into the silicon layer of the film rather than the metal-oxide layer of the film. The diffusion coefficients obtained with these measurements are in nearly perfect agreement with those reported by Cowern et al [4].

However, there remain many challenges in refining the thermal load given to the samples. In the vacuum tube furnace samples, there was measurable dopant diffusion, however there was significant surface degradation. This was also shown to be an issue for samples where RTA parameters were not perfectly controlled, as cracking developed on the surface. Once the RTA parameters were well controlled, the surface damage was minimized. Although the minimal thermal load tested did not result in substantial boron diffusion, this approach is clearly superior to the previously tested ones and can be further developed for high accuracy control of ultra-shallow doping.

Overall, this study combines the use of area-selective atomic layer deposition and dopant containing small molecule inhibitors to place dopant at precise locations.

Going forward, future efforts should be focused on finding a balance between thermal load, diffusion, and thin-film integrity. Furthermore, other model combinations of materials may be worth looking into. For example, using a different thin film with a more agreeable coefficient of thermal expansion to better match that of silicon, such as hafnia, could be utilized. Lastly, efforts can be made to measure the conductivity of samples doped in this manner to view carrier activation.

REFERENCES

1. Bansal, A., Li, X., Yi, S. I., Weinberg, W. H., & Lewis, N. S. (2001). Spectroscopic studies of the modification of crystalline si(111) surfaces with covalently-attached alkyl chains using a chlorination/alkylation method. *Journal of Physical Chemistry B*, *105*(42), 10266–10277. https://doi.org/10.1021/jp010284p

2. Byron, C., Silva-Quinones, D., Sarkar, S., Brown, S. C., Bai, S., Quinn, C. M., Grzenda, Z., Chinn, M. S., & Teplyakov, A. v. (2022). Attachment Chemistry of 4-Fluorophenylboronic Acid on TiO2and Al2O3Nanoparticles. *Chemistry of Materials*, *34*, 10659–10669. https://doi.org/10.1021/acs.chemmater.2c02789

3. Cardon, J. M., Krueper, G., Kautz, R., Fabian, D. M., Angsono, J., Chen, H.-Y., & Ardo, S. (2021). Reconciliation of Differences in Apparent Diffusion Coefficients Measured for Self-Exchange Electron Transfer between Molecules Anchored to Mesoporous Titanium Dioxide Thin Films. *ACS Applied Materials & Interfaces*, *13*(35), 41396–41404. https://doi.org/10.1021/acsami.9b19096

4. Cowern, N. E. B., Simdyankin, S., Ahn, C., Bennett, N. S., Goss, J. P., Hartmann, J.-M., Pakfar, A., Hamm, S., Valentin, J., Napolitani, E., de Salvador, D., Bruno, E., & Mirabella, S. (2012a). *Extended point defects in crystalline materials: Ge and Si*. https://doi.org/10.1103/PhysRevLett.110.155501

5. Dorn, R. W., Ryan, B. J., Lamahewage, S. N. S., Dodson, M. v., Essner, J. B., Biswas, R., Panthani, M. G., & Rossini, A. J. (2023b). Chlorination of Hydrogenated Silicon Nanosheets Revealed by Solid-State Nuclear Magnetic Resonance Spectroscopy. *Chemistry of Materials*, *35*, 539–548. https://doi.org/10.1021/ACS.CHEMMATER.2C02980

6. Haber, J. A., & Lewis, N. S. (2002). Infrared and X-ray photoelectron spectroscopic studies of the reactions of hydrogen-terminated crystalline Si(111) and Si(100) surfaces with Br2, I2, and ferrocenium in alcohol solvents. *Journal of Physical Chemistry B*, *106*(14), 3639–3656. https://doi.org/10.1021/jp0102872

7. Jain, S. C., Schoenmaker, W., Lindsay, R., Stolk, P. A., Decoutere, S., Willander, M., & Maes, H. E. (2002). Transient enhanced diffusion of boron in Si. *Journal of Applied Physics*, *91*, 8919–8941. https://doi.org/10.1063/1.1471941

8. Kern, W. (1990). Evolution of silicon wafer cleaning technology. *Proceedings - The Electrochemical Society*, *90*, 3–19. https://doi.org/10.1149/1.2086825

9. Kirchhof, J., Unger, S., Klein, K. F., & Knappe, B. (1995). Diffusion behavior of fluorine in silica glass. *Journal of Non-Crystalline Solids*, *181*, 266–273. https://doi.org/10.1016/S0022-3093(94)00525-7

10. Lai, M., Wei, L., Huang, Y. H., Wang, X. D., & Yang, Z. (2024). Revisiting the Influence of Surface Alkoxylation on Colloidal Silicon Nanocrystals. *ACS Photonics*, *11*, 2439–2449. https://doi.org/10.1021/acsphotonics.4c0033510

11. Lu, W., & Lieber, C. M. (2007). Nanoelectronics from the bottom up. *Nature Materials*, *6*, 841–850. https://doi.org/10.1038/nmat2028

12. Moore, G. E. (2009). Cramming more components onto integrated circuits, Reprinted from Electronics, volume 38, number 8, April 19, 1965, pp.114 ff. *IEEE Solid-State Circuits Society Newsletter*, *11*, 33–35. https://doi.org/10.1109/n-ssc.2006.4785860

13. Pi, X. D., Burrows, C. P., & Coleman, P. G. (2003). Fluorine in Silicon: Diffusion, Trapping, and Precipitation. *Physical Review Letters*, *90*, 4. https://doi.org/10.1103/PhysRevLett.90.155901

14. Silva-Quinones, D., Butera, R. E., Wang, G. T., & Teplyakov, A. v. (2021). Solution Chemistry to Control Boron-Containing Monolayers on Silicon: Reactions of Boric Acid and 4-Fluorophenylboronic Acid with H- And Cl-terminated Si(100). *Langmuir*, *37*, 7194–7202. https://doi.org/10.1021/acs.langmuir.1c00763

15. Silva-Quinones, D., Mason, J. R., Norden, R., & Teplyakov, A. v. (2024). Inhibition of atomic layer deposition of TiO2 by functionalizing silicon surface with 4-fluorophenylboronic acid. *Journal of Vacuum Science & Technology A*, *42*. https://doi.org/10.1116/6.0003316

16. Song, S. K., Saare, H., & Parsons, G. N. (2019). Integrated Isothermal Atomic Layer Deposition/Atomic Layer Etching Supercycles for Area-Selective Deposition of TiO2. *Chemistry of Materials*, *31*, 4793–4804. https://doi.org/10.1021/acs.chemmater.9b01143

17. Taiwan Semiconductor Company. (n.d.). *3nm Technology*. Https://Www.Tsmc.Com/English/DedicatedFoundry/Technology/Logic/L_3nm.

Appendix A

Tube Furnace Annealed Samples Large Area AFM

15 Minute

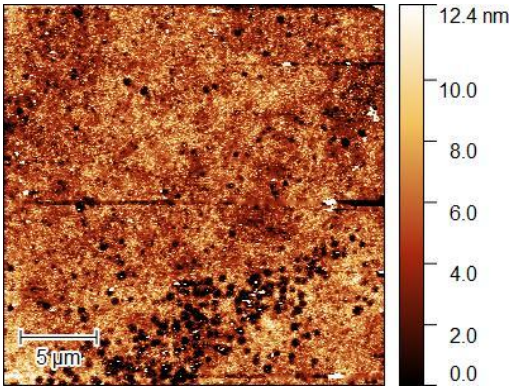

30 Minute

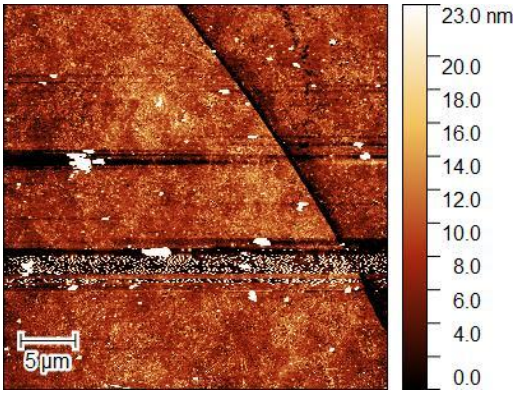

Appendix B

First Rapid Thermal Annealing Large Area AFM Images

Sample 1

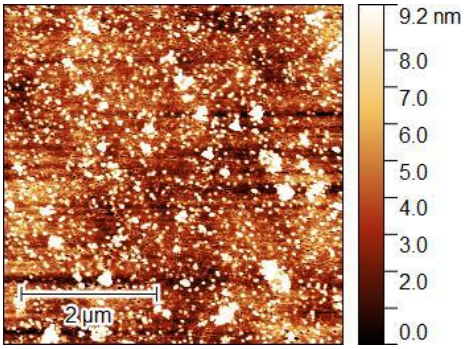

Sample 2

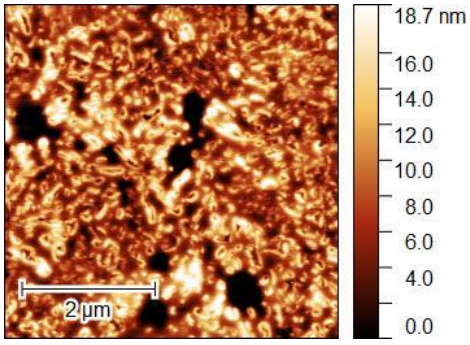

Sample 3